Investigating the Co-precessing Frame Approximation for Binaries on Eccentric Orbits

Sam Johar, Taylor Knapp, Lucy Thomas
(Dated: August 14, 2025)

Quasi-circularity has historically been assumed for detected gravitational waves from black hole compact binary coalescences (CBCs). As detector low-frequency sensitivity improves, we expect to detect CBCs from farther before merger, before eccentricity has been radiated away. To analyze these signals, we will need well developed and robust eccentric models. Few existing models incorporate precession and eccentricity together as waveforms resulting from this combination of effects are complex and difficult to model. The co-precessing frame is one tool that simplifies precessing waveforms by creating a reference frame in which the z-axis is always aligned with orbital angular momentum, a transformation that is well-studied for quasi-circular systems and often used to create precessing waveform models. Here we evaluate the co-precessing frame approximation for eccentric and precessing systems using numerical relativity simulations. We find that, while shifting to the co-precessing frame counteracts amplitude modulation in the waveform envelope, mode asymmetries caused by precession remain in the untwisted waveform. The determination of which precession features are not affected by the co-precessing frame transformation will aid in future efforts to construct a robust waveform model that includes the effects of both eccentricity and precession.

I. INTRODUCTION

Analysis of current LIGO data assumes that the orbit of a binary black hole (BH) system is quasi-circular. However, as detector sensitivity increases, we are more likely to begin observing eccentricity in detected waveforms. Part of the reason that LIGO detectors have not yet identified a non quasi-circular system is that eccentric binaries tend to circularize over time as gravitational waves emitted by the system radiate away eccentricity by removing excess angular momentum from the system. This circularizing effect can be seen in Figure 1, which depicts the inspiral of a low eccentricity waveform model. As detectors become more sensitive in the low frequency range (20Hz-50Hz), the inspirals of detected compact binary coalescences (CBCs) will be better resolved, giving us a better chance of seeing eccetricity before it has been radiated away. Additionally, now that we have identified many CBCs and analyzed them under the assumption of quasi-circularity, we are in a better position to relax this assumption going forward.

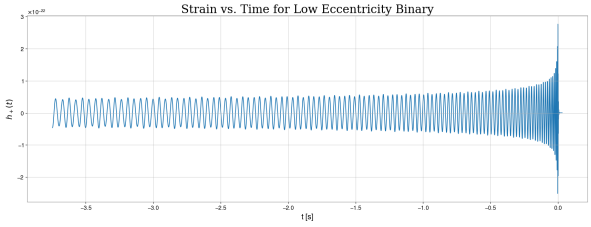

FIG. 1. Plus polarization of strain over time for the inspiral of a BH binary with 0.05 eccentricity. At the beginning of the inspiral, the periodic higher amplitude "knocking" characteristic of an eccentric system is clearly visible. One such knock can be seen just before the -3.5 second mark. However, these knocks become less clearly distinguishable throughout the inspiral. This waveform was generated with the LIGO Algorithm Library Simulation (LALSimulation) code package [1].

Binary black hole systems form in two main ways: isolated formation and dynamical capture. Isolated binaries are systems where the two bodies were orbiting each other in a binary before becoming black holes, while dynamical systems form when two pre-existing black holes approach each other, usually in a globular cluster, and are caught in each others' gravitational pull [2]. In isolated systems, we expect the orbit to be quasi-circular. However, we expect that dynamical systems could have eccentric orbits, in part because the binary will not have had as much time to radiate away eccentricity. Thus, detecting eccentric waveforms would provide evidence towards such systems being formed via dynamical capture. Modelling eccentricity allows researchers to stop making the assumption of quasi-circularity and will ensure that the tools exist to analyze eccentric waveforms when we eventually observe them.

Eccentricity (e) varies from 0 to 1 for bound systems, with e = 0 representing a circular orbit and e = 1 a parabolic orbit. In a quasi-circular orbit, each black hole has a constant angular velocity throughout one orbit. However when e > 0 and the orbit is elliptical, a black hole's angular velocity varies depending on the location in its orbit. At the point where the two black holes are closest together, known as **periastron**, the black holes travel with the fastest angular velocity and emit the highest amplitude GWs. Conversely, their angular velocity is slowest when they are farthest away from each other at **apastron**, and they emit lower amplitude GWs. These amplitude changes modulate the signal, creating periodic "knocks" at periastron[3]. Binaries with elliptical orbits will also experience **periastron precession**, an effect predicted by general relativity wherein an object's orbit itself precesses around the focus of its orbital ellipse within the orbital plane. This precession is due to ellipticity, and is not related to spin.

Taking into account the spins of the black holes in a CBC further complicates the observed GW. General relativity predicts that spinning objects affect the curvature

of spacetime by "dragging" the space around them[4]. In a binary black hole system, we denote the orbital angular momentum vector $\vec{L}$. This vector is by definition always perpendicular to the instantaneous plane of orbit. When the spins of the black holes are parallel or anti-parallel to $\vec{L}$, the system has **aligned spins** and both the spins and orbital angular momentum remain fixed in direction[5]. Systems with aligned spins have been well modelled and investigated[6].

However, if the spins are not aligned with $\vec{L}$, the system is complicated by a precession effect known as **Lense-Thirring Precession**, which has been observed in detector data. Due to general relativity, a spinning black hole will drag the space around it within the plane of orbit, affecting the GWs it emits. This dragging effect creates spin-orbit and spin-spin couplings, leading both the orbital plane (and thus $\vec{L}$) and the spins of the black holes themselves to precess[4]. Precession leads to modulation of the signal's amplitude and frequency as the alignment of the incoming GW with respect to the detector changes with $\vec{L}$, an effect that is demonstrated by Figure 2. The phase of the precessing waveform is also modulated, though this effect is more difficult to observe in the plot. Figure 3, which is Figure 1 in Shaikh 2025 [7], uses numerical relativity (NR) simulations to depict the effects of eccentricity and precession on a waveform in the time-domain.

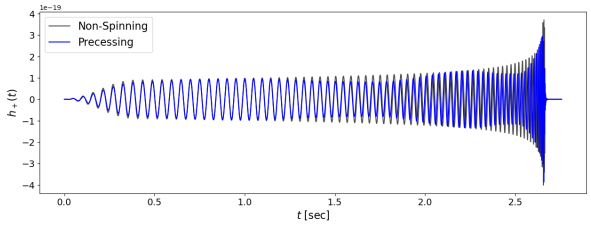

FIG. 2. Plus-polarization of strain over time for the inspiral of a precessing waveform (blue) and non-precessing waveform (grey). Amplitude modulation of the precessing waveform is clearly visible in contrast to the smooth amplitude increase in the non-precessing waveform. The two waveforms are roughly the same length, indicating that precession does not affect inspiral duration. Both waveforms were generated with LALSimulation [1].

Another effect caused by precession is mode asymmetry. In a non-precessing waveform, the following equation holds for each (ℓ,m) mode:

$$h^{\ell,m} = (-1)^{\ell}\bar{h}^{\ell,-m}. \quad (1)$$

[8] Thus, for a non-precessing system, the amplitudes of corresponding (ℓ,m) and (ℓ,-m) modes are the same. However, in a precessing system, spin-orbit couplings between the black holes and the orbital plane cause a breakdown in these symmetries on the orbital timescale as the orbital plane itself is precessing *during* each orbit and

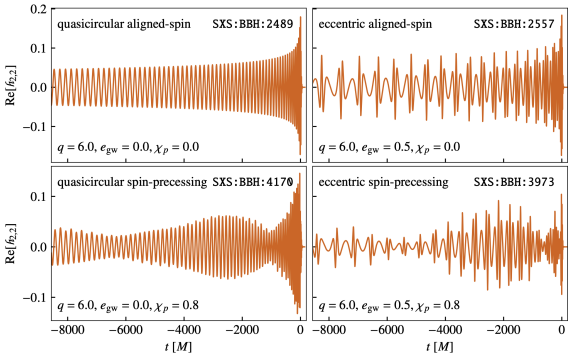

FIG. 3. [7]

thus symmetry across the orbital plane during each orbit is lost. Overall, precession complicates a GW by modulating its amplitude and phase and creating mode asymmetries.

One tool to simplify the complex waveforms from precessing systems is the **co-precessing frame** ([9][10][11]). The co-precessing frame is the reference frame that rotates with $\vec{L}$ such that $\vec{L}$ is always in the +z direction. Within the co-precessing frame, the complex seven-dimensional parameter space of a precessing system is reduced to a two-dimensional space built on waveforms that do not precess. One way to shift into this frame is to characterize the precessing system by describing $\vec{L}$'s position with respect to each axis with three time-dependent rotation angles, the most important of which is $\beta(t)$: the angle between $\vec{L}$ and the +z axis in the lab frame. Shifting into the co-precessing frame forces $\beta(t) = 0$, simplifying the system as described by Schmidt et al [6]. We utilize the minimal rotation condition version of the co-precessing frame, which enhances this technique by uniquely defining the rotation operator as described in Boyle et al. 2011 [12].

The co-precessing frame approximation treats this tool as a technique that removes precession effects from a waveform, leaving a signal that could have resulted from a non-precessing system. However, while shifting to this frame greatly reduces effects such as amplitude modulation by ensuring that $\vec{L}$ and $\hat{z}$ are always aligned, this approximation is not perfect. In particular, the mode asymmetries created by precession are features that cannot be removed with the co-precessing frame transformation (nor in any other frame), as proven in Section IIB of Boyle et al. 2014 [8].

Inspiral-merger-ringdown (IMR) models for quasi-circular precessing systems are mature and have been used extensively for GW data analysis. IMR models with eccentric inspirals have also been used for data analysis more recently, but these models do not include eccentricity in the merger or ringdown phase—a fairly accurate approximation as a binary typically circularizes before the merger stage. Eccentric and precessing inspiral models using Post-Newtonian (PN) approximations

exist, but no well-reviewed or tested eccentric and precessing IMR models exist as of yet. The closest current model [13], which is in early stages of development, has not yet been reviewed. This model uses the co-precessing frame approximation to construct eccentric and precessing IMR waveforms. However, while the impacts of the co-precessing frame on quasi-circular binaries has been widely reviewed, this "untwisting" effect has not been well studied for waveforms that are both eccentric and precessing.

Our objective is to study the co-precessing frame as a tool to remove precession effects for eccentric waveforms. We hope to determine the accuracy of this approximation in removing precession effects from eccentric waveforms by comparing untwisted eccentric precessing and eccentric non-precessing waveforms. In particular, we will try to explain and characterize flaws in this approximation by studying mode asymmetries in the waveforms. We begin with a brief overview of our motivations in Section II. Keeping these goals in mind, we introduce our methods in Section III. In Section IVA, we present an initial analysis of the effect of changing five parameters (total mass, mass ratio, aligned spin, precession, and eccentricity) on a waveform, as well as the effect of precession, eccentricity, and mass ratio on mode hierarchy. In Section IVB, we present results from our exploration of the motion of orbital angular momentum vector $\vec{L}$ for waveforms of varying eccentricity and precession. In Section IVC, we begin investigating the co-precessing frame by transforming two NR waveforms and comparing the resulting time-domain waveform and waveform modes to their inertial frame counterparts to observe the effect of the transformation. We build on this investigation in Section IVD, where we compare untwisted eccentric precessing waveforms to eccentric non-precessing waveforms to show that the co-precessing frame does not affect mode asymmetries. Section V details our proposed next steps for this project, both immediate goals like quantitative comparisons and long-term plans to construct a robust eccentric precessing waveform model using NR surrogates.

II. OBJECTIVES

Determining a relationship between eccentric and precessing waveforms and quasi-circular eccentric waveforms through the co-precessing frame allow us to construct a waveform model that includes eccentricity and precession. If we are able to determine a map between precessing and non-precessing waveforms, this future model could begin by creating non-precessing eccentric waveforms, then add in precession by "twisting" up with the inverse of the co-precessing frame approximation—an easier alternative to the complicated physics needed to model eccentric and precessing waveforms otherwise. We could then add in effects such as mode asymmetries, which our study shows are not created by the co-precessing frame transformation alone. Having such a model will increase our ability to identify future GW detections as eccentric and precessing.

III. METHODS

We begin by identifying the 28 eccentric and precessing waveforms simulations from the SXS catalog [14], where minimum eccentricity to be considered is e=0.01. Due to a lack of comparable non-precessing waveforms in the catalog, we use a combination of an eccentric non-spinning Numerical Relativity (NR) surrogate [15] and the SEOBNRv5EHM model [16] to generate a set of non-precessing waveforms for comparison. These waveforms have no precession, but otherwise the same parameters as the original eccentric and precessing waveforms. We then transform the 28 SXS simulations into the co-precessing frame using the scri code [11], and compare each resulting "untwisted" waveform to its non-precessing counterpart. This comparison will be done quantitatively (by eye with plotting) and qualitatively (by calculating the mismatch between each pair of waveforms), both in the time domain and looking at particular modes with a focus on the presence of mode asymmetries. We will also do a similar analysis for some eccentric and precessing waveforms generated by the Post-Newtonian code pyEFPE [17], and orbit-averaged code that does not depict mode asymmetries even in the inertial frame.

By comparing each "untwisted" waveform to an eccentric non-precessing counterpart, both qualitatively and quantitatively, we can determine how well the transformation removes precession effects. In particular, we can determine which effects it does *not* remove, especially by examining the presence of mode asymmetries in "untwisted" waveforms as compared to non-precessing ones.

Additionally, by comparing the efficacy of the transformation in removing precession between the three different waveform generation methods, we can evaluate each code package's accuracy as a model. In particular, since NR makes fewer approximations about the motion of binary objects, we can use comparison between executing this approach for PN pyEFPE waveforms and the NR simulations to see if there is missing physics in the PN code. For example, NR simulations are accurate enough to depict the mode asymmetries caused by precession, while pyEFPE does not–in fact, it is orbit averaged, so all effects that occur during an orbit are lost. Thus, if the co-precessing frame approximation yields better results for pyEFPE than the NR simulations and surrogates, we can infer that the missing physics in a non-precessing waveform as compared to an untwisted precessing one is on the orbital timescale.

IV. INTERIM RESULTS

We begin by changing different parameters to observe the resulting effects on GWs. Our observations from this

analysis are discussed in Section IV A. We gain initial familiarity with the dynamics of eccentric precessing waveforms using an orbit-averaged PN code [18], making plots to observe how eccentricity and precession affect their inspirals in Section IV B. In Section IV C, we detail our investigation of the parameters and characteristics of the 28 existing eccentric precessing NR waveform simulations from the SXS catalog in the inertial and co-precessing frames. We then lay out some plots and qualitative observations from our preliminary comparisons of NR simulations.

A. Effect of Changing Parameters on Time-Domain Waveforms

We present our findings from changing five parameters in Table I. We also present findings for how changing eccentricity and precession in particular affects mode hierarchy in Table II, and a corresponding plot in Figure 4. In our study, we primarily work with time-domain waveforms and waveform modes. Thus, by studying the effects of changing the following parameters on the visual appearance of a waveform, we gain insight into the expectations or "norm" for such waveforms, and an intuition for which effects result in which features on a signal.

Parameter	**Effect of Increasing Parameter on Time-Domain Waveform**
Total Mass	Inspiral shortens and amplitude increases
Mass ratio	Inspiral lengthens and amplitude decreases
z-axis spin	Inspiral lengthens
Precession	Amplitude and frequency modulate
Eccentricity	Inspiral shortens, amplitude (at periastron) increases, "knocking" effect (uneven amplitude per period)

TABLE I. Summary of investigation into effect of increasing five parameters on time-domain waveforms. Investigation run by creating waveforms with PN code [18]

Parameter	**Effect of Parameter on Mode Hierarchy**
Control (Non-spinning, quasi-circular, q = 1)	(2,2) mode is strongest, (2,1) and (3,3) modes are zero.
Precession	Adds power to (2,1) mode.
Eccentricity	Adds power to (3,3) and (2,1) modes.
Mass ratio	Adds power to (3,3) mode.

TABLE II. Effect of precession, eccentricity, and mass ratio on waveform mode hierarchy. Results for first three rows are displayed in Figure 4.

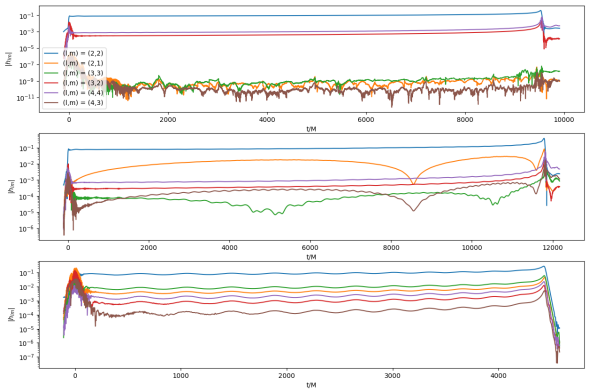

FIG. 4. Strain vs. time for six modes in control simulation, eccentric simulation, and precessing simulation. The mode hierarchy for the control simulation in order of decreasing amplitude is (2,2) (4,4) (3,2) (3,3) (2,1) (4,3). The precessing waveform adds power to the (2,1) mode, which becomes the second strongest. The eccentric waveform adds power to the (3,3) and (2,1) modes, which become the second and third strongest respectively. Plots were generated using NR simulations from SXS catalog[14].

B. PN Investigation of Eccentric and Precessing Waveforms

Using the eccprec PN code, we generate waveforms with varying precession and eccentricity respectively. As this code is orbit-averaged, the dynamics it outputs are missing complexity on the orbital timescale, making it difficult to fully analyze eccentric precessing waveforms with this code. However, it presents a computationally inexpensive way to model the macro shape of dynamics without orbital effects. In particular, we use this code to plot β(t), which is the angle of the orbital angular momentum $\vec{L}$ from the z-axis as a function of time (assuming $\vec{L}$ begins aligned with **z**). Figure 5 depicts the effect of increasing misaligned spin upon β(t), showing how systems with higher misaligned spin take the same amount of time to merge, but their orbital planes precess at a greater angle around total angular momentum $\vec{J}$. Figure 6 shows how $\beta(t)$ varies with eccentricity, with higher eccentricity systems merging faster and having higher amplitudes.

C. NR Simulations

By filtering the SXS catalog we find 28 waveforms that are both eccentric and precessing, or 19 waveforms if we remove those which are deprecated. We define eccentric to mean $e > 0.01$ and precessing to mean $\chi_{1_{perp}} + \chi_{2_{perp}} > 0.05$. We use scri to untwist these waveforms to the co-precessing frame and examine the results. In particular, we begin by qualitatively checking that the transformation decreases precession effects by comparing mode strength in the inertial and co-precessing

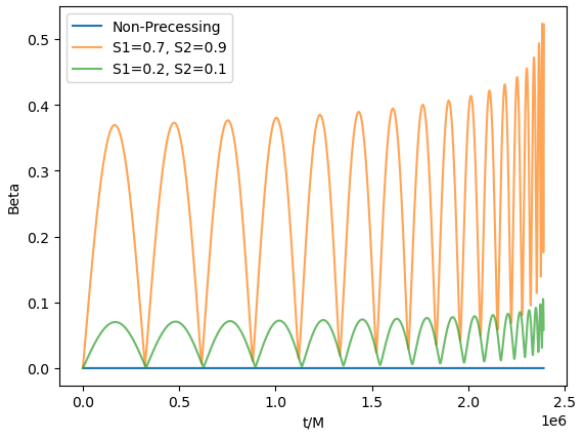

FIG. 5. Angle of $\vec{L}$ away from $\hat{z}$ (Beta) over time for systems with varying amounts of misaligned spin. All spins are in in the -x direction, and all waveforms are equal mass with $e = 0.1$. The non-spinning waveform (blue) always has $\beta = 0$, indicating that the orbital plane does not precess. The mildly spinning system (green) precesses at a lower angle than the highly spinning one (orange). Tracing the lower envelope of each line shows the evolution of total angular momentum $\vec{J}$ over time, which diverges farther from $\hat{z}$ for more highly precessing systems. Waveforms generated with PN code from [18] and starting frequency 10 Hz.

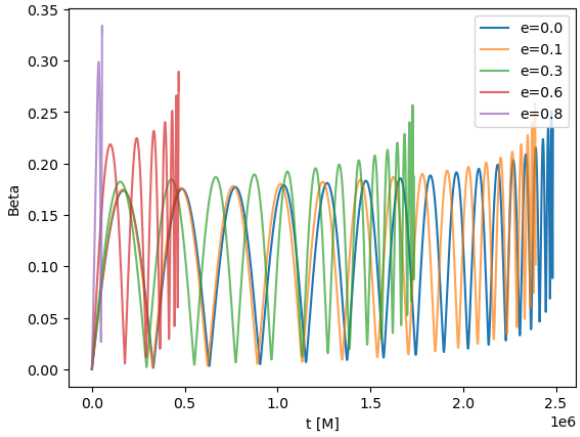

FIG. 6. Angle of $\vec{L}$ away from $\hat{z}$ (Beta) over time for systems with varying amounts of eccentricity. All waveforms are from equal mas systems with $S_{1_x} = -0.25$ and $S_{2_x} = -0.5$, and all other spin components are zero. More eccentric systems merge faster and reach higher precession angles. Tracing the lower envelope of each line shows the evolution of total angular momentum $\vec{J}$ over time, which does not vary with eccentricity. Waveforms generated with PN code [18] and starting frequency 10 Hz.

frames, as depicted for SXS:BBH:3725 in Figure 7. We find that transforming to the co-precessing frame does dampen the (2,1) mode, making the waveform closer to one from a non-precessing system. We start by focusing on SXS:BBH:0088, which is an equal mass system with an eccentricity of 0.074 and one black hole spinning with $\chi_p = 0.5$. We plot the waveform from an edge-on view, as this perspective should yield no cross polarization strain in a non-precessing waveform (Figure 8). The transformation to the co-precessing frame does flatten the cross polarization of the waveform to almost zero. The effect on the plus polarization is more difficult to see, but the residual shows how the waveform's amplitude is smoothed out in the co-precessing frame.

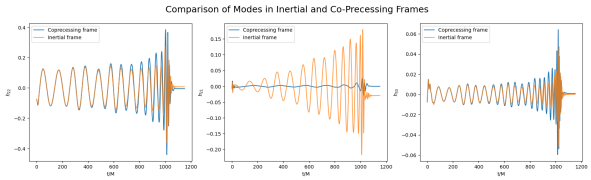

FIG. 7. Strain of (2,2) (2,1) and (3,3) modes over time in inertial (orange) and co-precessing (blue) frames for SXS:BBH:3725, a strongly eccentric and precessing waveform. In the co-precessing frame, the (2,1) mode is dampened to an amplitude much closer to what one would expect from a non-precessing waveform. As power is taken away from the (2,1) mode, the (2,2) and (3,3) modes gain power. Additionally, the amplitude increase of the (2,2) mode as the system approaches merger is smooth (apart from knocks due to eccentricity) in the co-precessing frame. Waveforms accessed from the SXS Catalog [14].

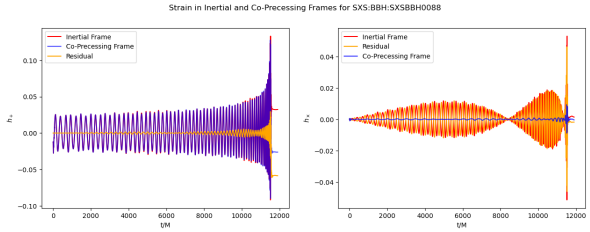

FIG. 8. Strain plus and cross polarization over time in inertial (red) and co-precessing (blue) frames for SXS:BBH:0088, plotted with the residual of those two quantities as a function of time. Waveforms accessed from the SXS Catalog [14].

D. Initial Co-Precessing Frame Comparisons

We implemented a code that filtered the entire SXS catalog to find "matches" to the 28 eccentric precessing waveforms. On our first run, we set the following parameters to be considered a match, where the "ep" supscript denotes eccentric precessing waveforms and the "match" subscript denotes a corresponding ec-

centric non-precessing waveform:

$$|\chi_{eff_{ep}} - \chi_{eff_{match}}| < 0.1$$
$$|q_{ep} - q_{match}| < 0.4$$
$$|\Omega_{ep} - \Omega_{match}| < 0.0005$$
$$0.7 < \frac{e_{ep}}{e_{match}} < 1.3$$
$$|\chi_{1_{\perp_{match}}} + \chi_{2_{\perp_{match}}}| < 0.01$$

With these condition, we find only one match: SXS:BBH:0088 and SXS:BBH:2580. SXS:BBH:0088 is precessing and has non-negligible spin on m_1, with $\chi_{1_\perp}$ of around 0.50. Both CBCs are equal mass systems with a low starting eccentricity of around 0.074 and 0.091 respectively. They have similar initial orbital frequencies, though SXS:BBH:0088 has about 5 more orbits than its counterpart.

We untwist SXS:BBH:0088 into the co-precessing frame to compare it to its non-precessing counterpart in Figure 9. From initial qualitative comparisons, the transformation drastically lessens precession effects, making it more similar to a non-precessing waveform. In particular, the cross polarization of the strain is much closer to zero than in the inertial frame (as also shown in Figure 8). The half period offset in the knocks between the two waveforms is a result of a difference in mean anomaly, not an effect of the co-precessing frame transformation. However, small wiggles of modulating amplitude remain in the cross polarization of SXS:BBH:0088, unlike its non-precessing counterpart which has a completely flat cross polarization. These features cannot be explained by differences between the two waveforms' parameters, showing that the co-precessing frame does not completely erase precession effects.

To further investigate the differences between these waveforms, we plot the amplitudes of the (2,±2) modes of both simulations in the inertial frame, and of SXS:BBH:0088 in the co-precessing frame as well (Figure 10). While the (2,±2) modes have the same amplitude for the non-precessing SXS:BBH:2580, indicated that mode symmetries are upheld, they are offset from each other in phase for SXS:BBH:0088 in both the inertial and co-precessing frames. In the inertial frame, this mode asymmetry is an effect caused by precession of the orbital plane. Its presence in the co-precessing frame indicates that this transformation does not remove mode asymmetries caused by precession, instead just shifting the envelope of the waveform upwards to be in line with that of a non-precessing system.

V. CHALLENGES AND FUTURE STEPS

Though our initial hope was to do all our comparison plots using existing NR simulations, we are unable to due to the lack of matches within the catalog. To expain why

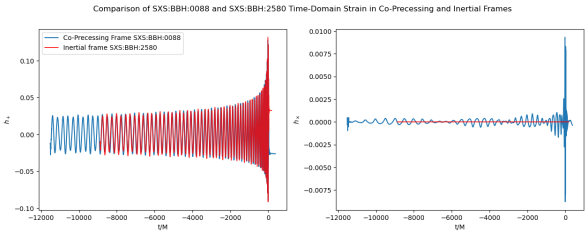

FIG. 9. Plus and cross polarization of strain as a function of time for SXS:BBH:0088 in the co-precessing frame and SXS:BBH:2580 in the inertial frame. The plus polarizations look similar, besides a half period offset caused by a difference in mean anomaly. However, there are small oscillations with modulated amplitudes on the precession timescale visible in the cross polarization, whereas for the non-precessing SXS:BBH:2580 no such oscillations are visible. This discrepancy shows that the co-precessing frame approximation does not fully hold; there are some effects that the co-precessing frame transformation does not change. Waveforms accessed from the SXS Catalog [14].

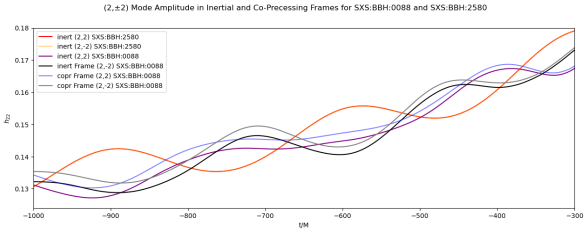

FIG. 10. (2,±2) mode amplitudes over time for eccentric precessing simulation SXS:BBH:0088 in the inertial and co-precessing frames and eccentric non-precessing simulation SXS:BBH:2580 in the inertial frame. The two mode amplitudes are the same for the non-precessing system. In both the inertial and co-precessing frames for the precessing system, the (2,2) and (2,-2) mode amplitudes are offset from each other in phase and amplitude, displaying that the mode asymmetry created by precession is not eliminated in the co-precessing frame. Waveforms accessed from the SXS catalog [14].

we cannot relax our matching parameters to continue our analysis using just SXS simulations (without surrogates), in Figure 11 we plot a "bad match" created by loosening the requirement for similar orbital frequency. While the two waveforms have very similar eccentricities, spins, and mass ratios, their differing starting orbital frequencies leads the eccentric non-precessing SXS:BBH:2536 to be much longer than its counterpart. As a result, the plus polarizations of their strains are difficult to compare and only line up in brief sections of the plot. Thus, to enable a proper comparison it is necessary to have closely matching waveforms and loosening our matching criteria would interfere with our ability to evaluate the co-precessing frame. In order to proceed with these comparisons, we will construct our own eccentric non-spinning waveforms with the same parameters as each eccentric precessing simulation from the SXS catalog. For

non-spinning waveforms with a mass ratio below 3.5 we construct these waveforms with an eccentric NR surrogate model [15], and for other waveforms we will use the SEOBNRv5EHM model [16].

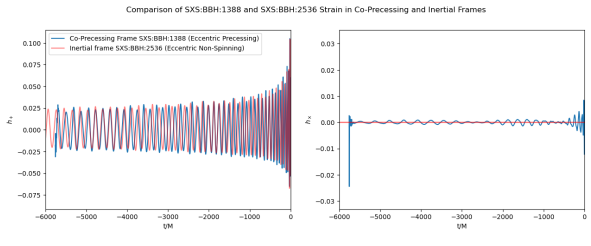

FIG. 11. Plus and cross polarization of strain as a function of time for SXS:BBH:1388 in the co-precessing frame and SXS:BBH:2536 in the inertial frame. Unlike for the "good" match from Figure 9, the two waveforms only line up at a few points during their orbits, and the co-precessing frame waveform is clearly higher frequency than its counterpart throughout. [14]

Moving forward, we will use mismatches to do quantitative comparisons of waveforms within the catalog. Using mismatches may help us identify a few more matches, and will add to our qualitative analysis of Figure 9. We will also use mismatches to compare our constructed eccentric matches to the eccentric precessing simulations, as well as plot the pairs together for qualitative analysis. These comparisons will help us evaluate the co-precessing frame to determine which precession effects it alters, and which it does not.

We will also perform the same comparisons on waveforms generated with pyEFPE code to see if the differences between eccentric non-precessing and untwisted eccentric precessing waveforms remain in a PN orbit-averaged code. Understanding the difference between eccentric waveforms and untwisted precessing waveforms will allow us to create a new eccentric precessing waveform model by twisting up eccentric NR surrogate waveforms and then separately adding in mode asymmetries and other physics we have determined is missing by our studying of the co-precessing frame.

[1] LIGO Scientific Collaboration, Virgo Collaboration, and KAGRA Collaboration, LVK Algorithm Library - LALSuite, Free software (GPL) (2018).

[2] M. Mapelli, Binary black hole mergers: Formation and populations, Frontiers in Astronomy and Space Sciences **7**, 10.3389/fspas.2020.00038 (2020).

[3] M. Favata, SXS, and K. Thorne, Elliptical binaries, Sounds of Spacetime (2025).

[4] T. A. Apostolatos, C. Cutler, G. J. Sussman, and K. S. Thorne, Spin-induced orbital precession and its modulation of the gravitational waveforms from merging binaries, Phys. Rev. D **49**, 6274 (1994).

[5] M. Favata, SXS, and K. Thorne, Spinning binaries, Sounds of Spacetime (2025).

[6] P. Schmidt, M. Hannam, and S. Husa, Towards models of gravitational waveforms from generic binaries: A simple approximate mapping between precessing and non-precessing inspiral signals, Phys. Rev. D **86**, 104063 (2012), arXiv:1207.3088 [gr-qc].

[7] M. A. Shaikh, V. Varma, A. Ramos-Buades, H. P. Pfeiffer, M. Boyle, L. E. Kidder, and M. A. Scheel, Defining eccentricity for spin-precessing binaries (2025), arXiv:2507.08345 [gr-qc].

[8] M. Boyle, L. E. Kidder, S. Ossokine, and H. P. Pfeiffer, Gravitational-wave modes from precessing black-hole binaries (2014), arXiv:1409.4431 [gr-qc].

[9] P. Schmidt, M. Hannam, S. Husa, and P. Ajith, Tracking the precession of compact binaries from their gravitational-wave signal, Phys. Rev. D **84**, 024046 (2011).

[10] R. O'Shaughnessy, B. Vaishnav, J. Healy, Z. Meeks, and D. Shoemaker, Efficient asymptotic frame selection for binary black hole spacetimes using asymptotic radiation, Physical Review D **84**, 10.1103/physrevd.84.124002 (2011).

[11] M. Boyle, Angular velocity of gravitational radiation from precessing binaries and the corotating frame, Physical Review D **87**, 10.1103/physrevd.87.104006 (2013).

[12] M. Boyle, R. Owen, and H. P. Pfeiffer, Geometric approach to the precession of compact binaries, Physical Review D **84**, 10.1103/physrevd.84.124011 (2011).

[13] S. Albanesi, R. Gamba, S. Bernuzzi, J. Fontbuté, A. Gonzalez, and A. Nagar, Effective-one-body modeling for generic compact binaries with arbitrary orbits (2025), arXiv:2503.14580 [gr-qc].

[14] The sxs catalog of simulations (2025).

[15] T. Islam, V. Varma, J. Lodman, S. E. Field, G. Khanna, M. A. Scheel, H. P. Pfeiffer, D. Gerosa, and L. E. Kidder, Eccentric binary black hole surrogate models for the gravitational waveform and remnant properties: Comparable mass, nonspinning case, Physical Review D **103**, 10.1103/physrevd.103.064022 (2021).

[16] A. Gamboa *et al.*, Accurate waveforms for eccentric, aligned-spin binary black holes: The multipolar effective-one-body model SEOBNRv5EHM, (2024), arXiv:2412.12823 [gr-qc].

[17] G. Morras, G. Pratten, and P. Schmidt, Improved post-Newtonian waveform model for inspiralling precessing-eccentric compact binaries, Phys. Rev. D **111**, 084052 (2025), arXiv:2502.03929 [gr-qc].

[18] K. S. Phukon, N. K. Johnson-McDaniel, A. Singh, and A. Gupta, Evolution of precessing binary black holes on eccentric orbits using orbit-averaged evolution equations, (2025), arXiv:2504.20543 [gr-qc].